JOURNAL OF APPLIED ELECTROCHEMISTRY **20** (1990) 269–280

Electrogenerative oxidation of model alcohols at packed bed anodes

JOHN C. CARD, STEPHEN E. LYKE, STANLEY H. LANGER*

Chemical Engineering Department, University of Wisconsin, Madison, Wisconsin 53706, USA

Received 22 December 1988; revised 5 June 1989

The electrogenerative oxidation of dissolved ethanol and 2-propanol in aqueous 1 to 3 M sulphuric acid electrolyte was investigated at several types of packed bed anodes in ion exchange membrane separated cells. The operation of these electrogenerative cells which incorporated a platinum-catalysed commercial oxygen gas-diffusion-type cathode is described. It appears that for dissolved normal primary alcohols composite Teflon–platinum fuel-cell-type electrodes favour aldehyde formation while 'platinum on graphite' electrodes favour carboxylic acid formation. Oxidation of dissolved 2-propanol could be controlled to give acetone exclusively.

Nomenclature

- A current accountability (see Equation 4) (%)
- d thickness of the packed bed (cm)
- F Faraday constant ($C\,mol^{-1}$)
- i current density ($A\,cm^{-2}$)
- I cell current (A)
- κ conductivity of the electrolyte ($\Omega^{-1}\,cm^{-1}$)
- N molar production rate ($g\,mol\,s^{-1}$)
- α charge transfer coefficient
- ε void fraction
- Φ potential in the electroyte phase (V)
- n number of electrons passed in the electrode reaction.

1. Introduction

A variety of electrochemical reactors have been shown to be operative in the electrogenerative mode, where favourable thermodynamics and kinetics are used to produce desired chemical products together with by-product d.c. electricity so that the need for an external power source is eliminated. Despite the attractive features of such systems there have been limitations, since most processes studied to date have involved gaseous or volatile materials reacting at catalytic flow-by electrodes [1, 2]. However, many candidates for electrochemical processing are either liquids of low volatility or solids most suited for dissolution in liquid electrolytes. The present investigation of electrogenerative oxidation reactions of some model alcohols at packed bed catalytic anodes was initiated to study pertinent aspects of operation and electrocatalysis in the liquid phase. Ethanol and 2-propanol were selected as representative primary and secondary alcohols.

The choice of alcohols here is related to the fact that they can serve as models for organic compounds of much higher molecular weight as well as the growing interest in these materials from biomass based conversions [3]. The advantages of packed bed electrodes include the significant expansion of electrode area into three dimensions. Heretofore most electrochemical packed beds described in the literature have been operated in the electrolytic mode with only occasional attention to preparative problems [4–7]. Furthermore, with the objective of establishing initial standards and criteria for performance, reversible systems have been principal objects of research. In these reversible electrochemical systems, electrocatalytic features have been of only limited concern.

Of the simple alcohols investigated here, ethanol has been of interest as a substrate for fuel cell operation [8, 9] but specific chemical manufacture has not been pursued since complete oxidation was desired. With ethanol the following simple reactions can occur at the anode

$$C_2H_5OH \longrightarrow CH_3CHO + 2H^+ + 2e \quad (1)$$

$$C_2H_5OH + H_2O \longrightarrow CH_3C(=O)OH + 4H^+ + 4e \quad (2)$$

$$C_2H_5OH + 3H_2O \longrightarrow 2CO_2 + 12H^+ + 12e \quad (3)$$

In electrogenerative operation, paths 1 and 2 are most desirable if either can be made selective. Complete oxidation according to Equation 3 is generally an undesired side reaction since it gives no desired chemical product. With a dissolved liquid substrate and packed bed configuration there is a wider spectrum of catalytic electrode choices, as will be demonstrated. These include supported catalysts, Teflon–catalyst mixtures and chemically modified catalyst structures, all of which can influence product selectivity.

* Author to whom correspondence should be addressed.

0021-891X/90 $03.00 + .12

Electrolytes have been limited to high conductivity aqueous sulphuric and perchloric acid solutions employed in a flow-through cell.

2. Previous work

A wide variety of electrochemical techniques has been used to study ethanol oxidation, including controlled potential electrolysis [10], a.c. differential capacitance [11], linear sweep voltammetry of adsorbed [12, 13] and bulk [14–17] ethanol, potentiostatic pulse [18], differential electrochemical mass spectroscopy [19, 20] and electrochemically modulated infrared reflectance spectroscopy [21].

Using linear sweep voltammetry, Sunderland *et al.* [12] found the reaction rate to be independent of pH, and approximately first order in ethanol concentration on bright platinum up to 0.5 M, after which it became zero order. With galvanostatic and chronopotentiometric methods, Rao and Roy [22] found that first order behaviour was extended to 1.5 M ethanol concentration on platinized platinum.

Matsui *et al.* [18] studied ethanol oxidation in 0.5 M H_2SO_4 on a roughened platinum electrode by the potentiostatic pulse method. In the potential range of 0.3 to 0.45 V (RHE), the observed Tafel slope was 0.133 V per decade at 0° C. The observed reaction order with respect to ethanol was 0.98 in the concentration range of 0.05 to 2 M when surface coverage, potential and pH were held constant. It was thus concluded that the reaction mechanism in this potential region involved a rate limiting ethanol dehydrogenation and adsorption step followed by a second dehydrogenation to form acetaldehyde. At potentials above 0.5 V, ethanol oxidation was inhibited by acetic acid, which was one of the oxidation products.

Numerous cyclic volammetric studies have also been conducted. Sokolova [23] postulated a diadsorbed intermediate in the ethanol oxidation scheme, based on cyclic voltammetric data with smooth platinum. This was disputed by Snell and Keenan [24, 25] who proposed single site ethanol adsorption with platinum surface oxides playing an important role in the mechanism. Sokolova *et al.* [17] also showed that acetaldehyde had no effect on the proceses of formation and removal of this oxide layer.

For 1-propanol oxidation, as in the case of ethanol, Sokolova [23, 26] proposed a mechanism involving a diadsorbed intermediate. No effect on the mechanism was observed [27] when the tempertaure was increased from 15 to 60° C.

Cyclic [23, 27–30] and potential sweep [30, 31] voltammetry have been used to investigate isopropanol oxidation. Most of these studies suggest the involvement of surface oxides in the mechanism.

The vapour phase electrogenerative oxidation of ethanol has been investigated in our laboratories [1]. Vapour streams from 25 vol % ethanol/water mixtures were oxidized on Teflon–platinum-black gas-diffusion electrodes (American Cyanamid LAA-25, 25 mg Pt cm^{-2}) in undivided cells with 3 M H_2SO_4 electrolyte to give acetaldehyde and some carbon dioxide byproduct as indicated by Equation 3. Single-pass conversions of up to 60% were demonstrated. A patent has been issued for this process [32]. Further work on this system [2] was reported. Electrodes similar to those in the above study [1] but with lower catalyst loading (9 mg Pt cm^{-2}) were employed in a divided cell (RAI Research R-4010 cation exchange membrane). Acetaldehyde current accountabilities of up to 60% were obtained at single-pass conversions of up to 40%. An optimum anode potential for acetaldehyde production of about 0.66 V (RHE) was observed; at higher anode potentials, carbon dioxide formation increased significantly. Very little carbon dioxide formation was observed with dissolved ethanol feed (1 M EtOH in 3 M H_2SO_4 anolyte) to the reactor as compared with vapour feed from a 50 or 75 vol % ethanol/water solution, although the resulting current was also decreased. It was also shown that undesirable carbon dioxide byproduct formation could be minimized by increasing the molar ethanol vapour feed to the reactor. Heating the feed vaporizer to increase the feed rate increased the fraction of the current generated which was associated with acetaldehyde production and substantially decreased that associated with CO_2 formation.

Vapour phase electrogenerative oxidation of neat 2-propanol vapour was also investigated as part of an earlier study [2]. Current densities of over 30 mA cm^{-2} were obtained. Both acetone and carbon dioxide production were observed.

3. Experimental

3.1. *Cell design*

To focus on the packed bed anode, we have employed an ion exchange membrane divided hybrid cell incorporating a well characterized efficient oxygen gas diffusion cathode of the free electrolyte type. The flow system employed is shown schematically in Fig. 1. The soluble substrates of interest were in excess and held in the concentration range of 0.25 to 0.5 M with emphasis on obtaining representative polarization data and product characterization. Conversions were small, so that concentration polarization is not of great concern. However, the effect of product accumulation has been given some attention and indicates some potential electrocatalytic problems in packed bed operation, which may merit consideration in electrocatalyst design in the future.

The arrangements and general circuitry are shown in Fig. 2. Several forms of packed bed anodes were investigated. One type of heavily catalysed bed was composed of five American Cyanamid AA-1 (9 mg cm^{-2} Pt each) electrodes separated with 80 mesh tantalum screens to maintain conductivity and facilitate contact between dissolved reactant and electrocatalyst. The AA-1 electrodes themselves are Teflon–platinum mixtures supported on tantalum screens [33]. The packed bed was mounted inside a circular electrolyte

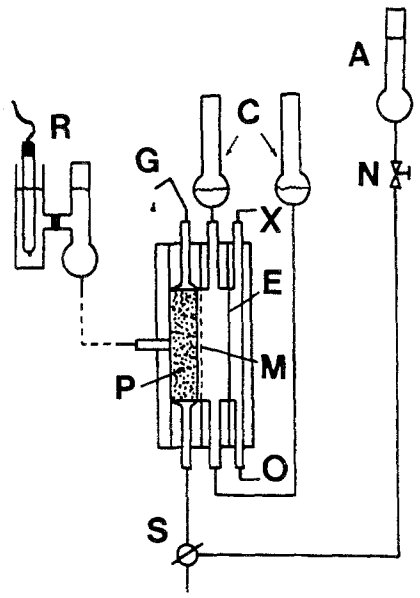

Fig. 1. Electrolyte flow system for packed bed cells. C = catholyte reservoirs, G = glass elbow for anolyte product recovery in a graduated cylinder (not shown), A = anolyte, R = calomel reference electrode in the reference reservoir, N = Teflon/glass needle valve, S = three-way stopcock, P = packed bed anode, E = gas diffusion oxygen cathode, M = membrane or separator, O = oxygen supply to cathode, X = excess oxygen to vent.

compartment in a configuration of the type used previously [2]. Either an American Cyanmid LAA-2 (9 mg cm^{-2} Pt) or LSE graphite electrode, both of which are porous to vapour, was employed at the exterior of the packed bed to recover vapour phase products during operation. A 45 mesh platinum current collector was located between the packed bed and anode gas diffusion electrode.

For other experiments, a new packed bed cell design was introduced. The cell configuration is indicated in

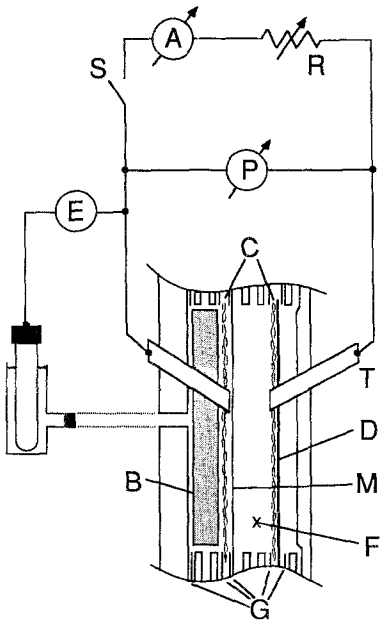

Fig. 2. Electrical system and schematic of rectangular cell with Pt-graphite anode. E = electrometer for measuing anode polarization against the reference electrode, S = switch, P = digital voltmeter, A = ammeter, R = variable external load resistance, B = packed bed anode, D = gas diffusion oxygen cathode, C = Pt screen current collectors, M = membrane or separator, G = Teflon/Viton gaskets, T = current collector tabs, F = free electrolyte cathode chamber.

Figs 1 and 2. Here the anode was platinum supported on porous graphite sheet although the same configuration was used for graphite felt or graphite particles. A catalyst loading of about 18 mg cm^{-2} was employed. The bed dimensions were 51 mm × 13 mm × 3.2 mm thick. In this cell, no Teflon–catalyst gas diffusion electrode was used with the packed bed anode. All anode operations took place completely in the liquid phase. A gas diffusion cathode of appropriate dimensions (51 mm × 13 mm) was employed. Electrolyte containing dissolved alcohol reactant (prepared immediately before the experiment) flowed up through the long bed dimension (51 mm). The bed thickness (3.2 mm) in the current flow direction (perpendicular to the electrolyte flow direction) was thin to minimize the ohmic drop across the anode. The Appendix includes a mathematical analysis that shows potential drop in the anolyte was probably small but not negligible under the reported experimental conditions. A platinum screen current collector was located at the front face of the bed facing the cathode, as indicated in Fig. 2.

In all reactor work, the oxygen counter electrode was an efficient American Cyanamid LAA-2 (9 mg cm^{-2} Pt). The LAA-2 is a gas-permeable electrolyte-impermeable electrode consisting of Teflon-bonded platinum black supported on porous tantalum screen and backed with a layer of porous Teflon [34] with approximately 1 μm pores. A cationic exchange membrane (RAI Research Raipore R-4010) was used to separate the two electrodes. The use of other membranes was also investigated. Nafion 117 showed performance similar to that of RAI R-4010. Nafion 324 exhibited better resistance to transport of acetic acid from the cathode, but had a much higher ionic resistance.

In both types of reactor some experiments were conducted with accommodations made for anode potential measurement against a calomel reference electrode containing saturated sodium chloride solution (SSCE). Since oxygen electrode polarization was reproducible to within about 10 mV, reference electrodes were not always used in the cell operation. In the packed bed cell employing AA-1 electrodes, a Luggin capillary was built into the packed bed compartment. This faced the gas diffusion electrode associated with the packed bed anode. In the Pt-graphite packed bed cell, a Teflon Swagelok tube fitting was mounted in the flat polypropylene plate at the rear of the packed bed (the side facing away from the cathode). Teflon tubing was used to connect the reference electrode vessel with the anode. The configuration is illustrated in Figs 1 and 2. A fine glass frit between the reference electrode and the cell prevented anolyte contamination from the SSCE.

3.2 *Packed bed electrode fabrication*

Several forms of graphite support were investigated in this study. Two graphite materials were obtained from the Electrosynthesis Co., East Amherst: graphite sheet (No. SG-13, 50% porosity, $\frac{1}{8}$ in thick) and graphite felt

(No. GF-S6 $\frac{1}{4}$in thick). High surface area porous graphite particles were also used (Superior Graphite Corp., Chicago: No. 9012 Desulco, 500 μm to 3.3 mm). Desulco grade graphite is very porous and of high purity (> 99.5% C, < 0.03% S). The particles were sieved to provide a uniform bed packing size of 0.84 to 1.0 mm. However, neither the graphite felt nor the graphite particles were particularly effective as catalyst supports compared to the graphite sheet using the preparative procedures and experimental techniques described here. Hence, work with the graphite sheet is emphasized.

In preparing the catalyst on the graphite sheet, the platinum was dispersed throughout the support by saturation with a 50 wt % aqueous solution of hydrogen hexachloroplatinate(IV) hydrate ($H_2PtCl_6 \cdot 4H_2O$) (Aldrich Chemical Co., Milwaukee). After this impregnation step and drying overnight at room temperature, the catalyst was placed in an oven for 45 min at 100° C. Residual water and chlorine were then removed from the electrode by heating at 250° C under a flowing hydrogen atmosphere for 3 h, leaving reduced platinum metal.

Using slow scan (0.5 V min^{-1}) voltammetry in the hydrogen adsorption region (−0.25 to 0.21 V w.r.t. SCE) it was possible to obtain a platinum surface area for some of the electrodes used here [35]. The Pt-graphite sheet electrode had a platinum area of about 500 cm^2 Pt (geom. cm)$^{-2}$, while that of each of the AA-1 electrodes was about 1500 cm^2 Pt (geom. cm)$^{-2}$. The total surface area of the Pt/graphite sheet catalyst was also determined using a flow-type BET surface area analyser (Micromeritics Flowsorb II 2300). The total surface area was 0.4 m^2 g^{-1} or 1600 true cm^2 (geom. cm)$^{-2}$.

3.3. *Electrode pretreatment*

In experiments involving the AA-1 packed bed, hydrogen gas was passed over the gas diffusion electrodes at the anode and cathode, while the cell was shorted for 30 min. After this time, the resistance across the unshorted cell was measured with a Keithley model 502 milliohmmeter.

In experiments involving the platinum/graphite packed bed, since no gas diffusion electrode was used in association with the anode, a different procedure was developed. Here, a constant current supply in series with an ammeter was connected across the cell. Also connected across the cell was a voltmeter. The current source (negative terminal connected to anode) was adjusted to maintain a cell potential of about 0 V, while hydrogen gas was fed to the cathode. A slight production of hydrogen gas bubbles at the anode was observed. Reduction was maintained under these conditions for about 40 min; the cell resistance was then measured with the Keithley milliohmmeter.

3.4. *Experimental procedures*

In all experiments, two polarization curves were performed for each set of experimental conditions. In the first curve, cell potential was changed every 4 min. In the second curve, cell potential was varied every 5 min and gas chromatographic analyses of the anode effluent gas (in cases where a gas diffusion electrode was present at the anode) were performed at the end of each 5 min period. For cell potentials that are reported as 'IR-corrected' the measured cell resistance with measured current was used to compensate for ohmic loss due to electrolyte and membrane resistances. When a reference electrode was included in the experiment, its potential relative to the reduced anode was recorded at the time of the reduction. This value was then used to refer potentials to the reversible hydrogen electrode (RHE).

Steady-state experiments were also performed. After data for the two polarization curves were obtained, the cell potential was adjusted to a region of interest and allowed to attain steady-state operation for about 25 min. After this period, samples of the anode effluent vapour were analysed by GC (in experiments where a gas diffusion type electrode was present at the anode) while a 5 to 10 ml sample of the anolyte effluent was obtained. This anolyte sample was immediately analysed using headspace chromatography. Other steady-state potentials were then investigated using the same procedure. The anolyte samples were refrigerated and analysed for dissolved acetic or propionic acid by HPLC either on the same day or the day following each experiment.

3.5. *Chemical analyses*

Gas chromatographic analyses of the anode effluent vapours during operation were accomplished on Carbowax 1540 (ethanol, acetaldehyde, ethyl acetate, 2-propanol, acetone), Porapak-Q (CO_2) and OV-101 silicone (ethyl acetate) columns using Carle model 8500 and 111 chromatographs. Head-space analyses were performed on electrolytes using the same columns. For the latter procedure, a small (200 μl) sample of the anolyte effluent was placed in a 50 ml Wheaton sealed (Teflon Mininert valve) vial and allowed to equilibrate for 25 to 40 min at room temperature before a sample of the vapour above it was withdrawn and analysed by gas chromatography. Calibration curves for several simulated liquid electrolyte standards bracketing the sample acetaldehyde or acetone vapour concentrations were performed on the same day in conjunction with the electrogenerative experiment.

The anolyte was also analysed with HPLC for acetic (ethanol experiments) and propionic (propanol experiments) acids using a derivative technique based on esterification with phenacyl bromide. The general procedure is described in the literature [36]. Electrolyte samples and standards were neutralized with KOH to pH 7, then derivatized in acetone–water solution with phenacyl bromide and triethylamine catalyst at 100° C for 75 min. Dilutions of the derivative in mobile phase (60/40 MeOH/H_2O for EtOH experiments and 40/60 MeOH/H_2O for PrOH experiments) were then analysed

at 254 nm with reverse phase chromatography (Econosphere ODS 25 cm).

Later a Hamilton PRP-X300 column was obtained so that electrolyte samples could be analysed directly. For this column samples and standards were neutralized with KOH to pH 2, diluted in mobile phase (10^{-2} M KH_2PO_4 for ethanol experiments and 95/5 10^{-3} M H_2SO_4/acetonitrile for propanol experiments) and injected onto the column directly.

4. Results

Electrogenerative oxidation of both model alcohols of this study in packed bed reactors produced steady-state currents in the range of 20 to 60 mA cm^{-2} at room temperature. Almost complete product recovery was achieved. Cell voltage corrected for IR loss was maintained generally above 200 mV to ensure that the anode potential did not rise above 750 mV w.r.t. RHE. This limit was based on previous experience since deterioration of catalytic properties had been observed. This deterioration was most probably due to formation of special oxides on the catalytic platinum surface. Initial results obtained with a circular AA-1 anode cell (of a type used earlier) are described below. Results from a more extensive study featuring rectangular platinum–graphite anodes are then presented. Use of platinum–graphite electrodes resulted in a different product selectivity and lower currents, but involved more efficient use of catalytic platinum surface area.

4.1. *AA-1 bed test cell*

The performance of the reactor incorporating the stacked American Cyanamid AA-1 Teflon–platinum electrodes is illustrated by the cell polarization curves of Fig. 3. The observed and IR-corrected cell potentials are plotted against current density based on apparent cross-sectional electrode area. Thus, current densities as high as 60 mA cm^{-2} were observed in this heavily catalysed bed (45 mg Pt cm^{-2}) which consisted of five stacked electrodes.

Steady-state experiments demonstrated that the major products were acetaldehyde and acetic acid

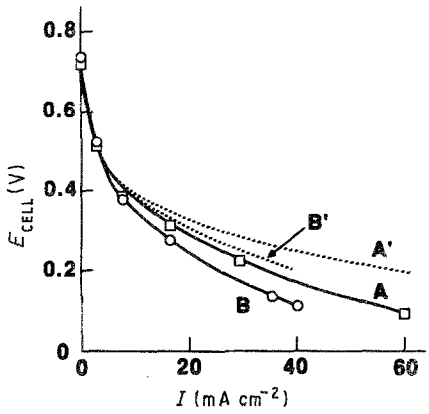

Fig. 3. Cell polarization curves for electrogenerative oxidation of dissolved ethanol in an AA-1 packed bed (with LSE electrode, see text). See Table 1 for experimental conditions. Curves A, A′ (Expt. 137): 0.5 M ethanol, T = 25° C, Cell R = 0.37 Ω. Curves B, B′ (Expt. 138): 0.25 M ethanol, T = 23° C, Cell R = 0.38 Ω. Curves A, B: observed potentials. Curves A′, B′: with IR correction.

produced in a ratio of approximately 5 to 2 as reflected in the current accountabilities of Table 1. Current accountability in this Table is defined as the fraction of observed cell current assigned to formation of each product relative to the total current. The assignment is based on observed products. Accountability is a measure of the selectivity of the electrode reaction. For example, current accountability for acetaldehyde, A_A, was calculated as

$$A_A = \frac{N_A F n}{I}(100\%). \qquad (4)$$

For the AA-1 packed bed, small amounts of acetaldehyde (5%) and CO_2 (see Table 1) were recovered in the nitrogen stream passed over the gas permeable LSE electrode located at the outside of the packed bed electrode. However, most of the acetaldehyde product remained dissolved in the flowing anolyte. This behaviour is similar to that observed in flow-past operation results reported earlier [2].

The AA-1 packed bed catalyst loading of 45 mg Pt cm^{-2} differed significantly from the 18 mg cm^{-2} loading of the Pt–graphite anodes used below. For purposes of comparison, turnover frequency was

Table 1. Selected steady-state data for ethanol oxidation; comparison of AA-1 and platinum–graphite anodes

Expt. *R* (Ω)	[*EtOH*] (M)	*Anode type*	*Anolyte flow* cm^3 min^{-1}	*Cell* (*mV*)	*Anode*[c] *E* (*mV w.r.t. RHE*)	*I* mA cm^{-2}	*% Current accountability*		
							AA	CO_2	*HOAc*
137 (0.37)	0.5	AA-1	0.7	188	637	57.4	63[a]	1	25
147 (0.31)	0.5	Pt–Gr	1.0	244	631	17.2	23	[b]	70
			0.9	204	666	20.0	26	[b]	70

[a] Acetaldehyde in Expt. 137 is total of that recovered in the nitrogen anode gas stream (5%) and that dissolved in the anolyte (58%) (see text).

[b] Carbon dioxide production could not be measured in the cell employing the Pt–graphite packed bed anode.

[c] Anode potential estimated from listed cell potential and oxygen cathode polarization data from other experiments.

AA = Acetaldehyde. HOAc = Acetic acid. Current accountability is defined in te text. R = Cell resistance. Anode type: AA-1 packed bed, geom. area = 5.07 cm^2; Pt–Gr = Pt–graphite packed bed, geom. area = 6.45 cm^2. Cell potentials are corrected for IR loss. Experiments in a divided cell (RAI R-4010 membrane) with LAA-2 oxygen cathode and 3 M H_2SO_4 electrolyte. T = 25° C.

used to measure the effectiveness of the use of the catalytic platinum surface. Based on the electrochemically measured surface area of the AA-1 electrode stack ($5 \times 1500\,cm^2$/apparent cm^2), the observed steady state product distribution and the current density of $57.4\,mA\,cm^{-2}$ (Table 1), an effective turnover frequency of $0.016\,s^{-1}$ could be calculated for the platinum electrocatalyst of the AA-1 packed bed.

4.2. *Platinum–graphite packed bed*

There was a marked difference in the product distribution obtained from the platinum–graphite packed bed compared with that from the AA-1 packed bed in similar steady-state experiments as shown in Table 1. While strong selectivity toward acetaldehyde was observed with the AA-1 packed bed, acetic acid (in the ratio of about 3 to 1 acetaldehyde) was the major product with the graphite supported platinum anode. Thus, the catalytic selectivity of the platinum-black/Teflon composite AA-1 electrodes is significantly different from that of the platinum–graphite packed bed. More will be said about this effect later.

Since the design of the Pt–graphite packed bed reactor involved an outer plastic face for support and incorporated no gas diffusion electrode for anode vapour product recovery, carbon dioxide production could not be monitored. However, on the basis of calculated current accountabilities for acetaldehyde and acetic acid, it appears that any CO_2 production was small. Results from two steady-state experiments with the platinum–graphite packed bed shown in Table 1 also demonstrate good reproducibility.

Turnover frequency calculated for the Pt–graphite electrode under the higher current conditions of Table 1 is $0.060\,s^{-1}$. By comparison, the analogous calculations already presented for the AA-1 bed gave $0.016\,s^{-1}$. Thus, although the AA-1 packed bed was quite active for electrogenerative oxidation of dissolved ethanol, the platinum–graphite packed bed involved more efficient use of platinum electrocatalytic surface sites. Efficient use of exposed platinum suggests that, with attention to catalyst dispersion, a graphite-supported catalyst packed bed configuration could be part of a cost-effective electrogenerative reactor design.

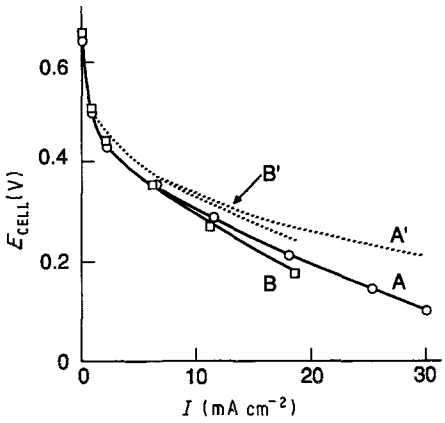

Fig. 4. Effect of ethanol concentration on cell polarization. Performance data for electrogenerative oxidation of dissolved ethanol in a Pt–graphite sheet packed bed. See Table 2 for experimental conditions. Curves A, A′ (Expt. 148): 0.5 M ethanol. Curves B, B′ (Expt. 153): 0.25 M ethanol. Curves A, B: observed potentials. Curves A′, B′: with IR correction.

The effectiveness of the electrogenerative packed bed reactor can be compared with conventional heterogeneous catalysis through the use of turnover frequencies. McCabe *et al.* [37, 38] developed alumina-supported platinum catalysts for ethanol oxidation and reported platinum surface as measured by CO chemisorption. From their data on 3 mm spheres with 0.1 vol % ethanol and 1 % oxygen feed at an hourly space velocity of 208, we can calculate turnover frequencies ranging from $0.3\,s^{-1}$ at 400 K to $1.1\,s^{-1}$ at 500 K. From these data, it can be seen that the electrocatalytic turnover is comparable at much lower temperatures and probably can be improved with further work at higher temperatures [12].

4.3. *Effect of reactant ethanol concentration*

The effect of dissolved ethanol concentration on the polarization behaviour of the Pt–graphite packed bed

Table 2. Selected steady-state data for ethanol oxidation at a platinum–graphite packed bed anode; effect of anolyte flow rate and ethanol concentration

Expt.	*[EtOH]* (M)	*Cell, R* (Ω)	*SS*	*Anolyte flow* $cm^3\,min^{-1}$	*Cell E* (*mV*)	*Anode*[a] *E* (*mV w.r.t. RHE*)	*I* $mA\,cm^{-2}$	*% Current accountability*	
								AA	*HOAc*
153	0.25	0.56	A	1.1	273	607	13.6	49	64
			B	1.7	276	602	14.5	53	69
			C	1.0	209	664	18.3	43	68
			D	1.6	227	645	18.5	40	62
148	0.5	0.56	E	1.0	274	600	17.5	30	81
			F	0.9	211	654	24.4	24	91

[a] Anode potential estimated from listed cell potential and oxygen cathode polarization data from other experiments.
AA = Acetaldehyde. HOAc = Acetic acid. Current accountability is defined in the text. R = Cell resistance. SS = Steady State. Pt–graphite packed bed anode, geom. area = $6.45\,cm^2$. Cell potentials are corrected for IR loss. Experiments conducted in a divided cell (RAI R-4010 membrane) with LAA-2 oxygen cathode and 1 N $HClO_4$ electrolyte. T = 26–28° C.

hybrid cell is shown in Fig. 4. While an increase in ethanol concentration from 0.25 M (Curve B) to 0.5 M (Curve A) resulted in a 50% increase in the maximum current density generated by the cell, still higher concentrations did not result in significant current increase. A similar effect was observed with the AA-1 packed bed (Fig. 3).

The effect of ethanol concentration on product selectivity is shown in Table 2. A comparison of steady states A and E indicates that selectivity toward acetic acid is enhanced when the reactant ethanol concentration in the anolyte is increased from 0.25 to 0.5 M. A comparison of steady states C and F is consistent with this observation.

4.4. *Effect of anolyte flow rate*

The flow rate of the anolyte containing the dissolved ethanol reactant appeared to have very little effect on product selectivity in the range investigated (1 to 2 $cm^3\ min^{-1}$). A comparison of steady states A and B in Table 2 demonstrates this point, as does a comparison of steady states C and D. Anolyte flow rate also had little effect on the current density generated (reaction rate). This result suggests that external mass transfer of ethanol from the bulk anolyte to the external anode electrocatalyst surface is not rate controlling [39]. The generated current in steady-state D of Table 2, for instance, only represents an approximate 7% conversion of dissolved ethanol to products. Mass transfer coefficients calculated from published correlations [40] for the conditions used here support this explanation.

Note that some of the calculated total accountabilities of Table 2 and other Tables discussed below exceed 100%. There are several possible reasons for this which will be discussed more extensively later. However, note that current accountabilities are based on three chromatographic analyses. The high totals could reflect common errors of the order of 5% in such analyses.

4.5. *Effect of electrolyte*

Another variable that was investigated was the type and concentration of the electrolyte used in the reactor (see Table 3). Although the less concentrated acid electrolytes exhibited lower ionic conductivity, as reflected in the higher values of measured cell resistance, no pronounced effect on product selectivity was observed. Perchloric acid electrolyte also provided reactor performance and operation similar to that observed with sulphuric acid (see Table 3).

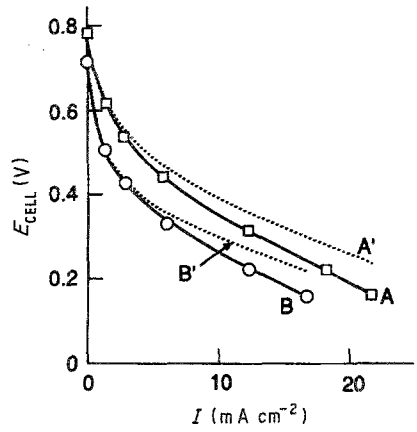

Fig. 5. IR-corrected polarization curves for electrogenerative oxidation of 0.5 M dissolved isopropyl alcohol (1 cc min^{-1}) in a Pt–graphite sheet packed bed. Electrode area = 6.45 cm^2, LAA-2 oxygen cathode, T = 26–28° C, Cell R = 0.45 Ω, electrolyte = 1 M H_2SO_4. Divided cell (R-4010 membrane). Expt. 154. Curves A, A′: without added acetone. Curves B, B′: with 0.1 M acetone added to the anolyte. Curves A, B: observed potentials. Curves A′, B′: with IR correction.

4.6. *Oxidation of dissolved 2-propanol*

With the demonstration of effective ethanol oxidation on the graphite-supported platinum packed bed anode it was of interest to compare operation with a simple secondary alcohol, e.g. 2-propanol. Figure 5 shows that current densities obtained with this alcohol were almost as high as those with ethanol. In Table 4, the results of operation at two steady states for each alcohol are presented.

Acetone product dissolved in the anolyte from the 2-propanol oxidation experiments was analysed with headspace chromatography, using a similar procedure to that for acetaldehyde. The value of 108% current accountability for acetone in Experiment 154 reflects the accuracy of the analysis, which was typically better than 20% for acetone and 10% for acetaldehyde. Interestingly, no propionic acid was produced from reaction of dissolved 2-propanol. In contrast, acetic acid was the major product from ethanol oxidation under similar operating conditions. This illustrates a

Table 3. Selected steady state data for ethanol oxidation at a platinum–graphite packed bed anode; effect of electrolyte type and concentration

Expt.	*[Acid]*	*Cell, R (Ω)*	*Anolyte flow $cm^3\ min^{-1}$*	*Cell E (mV)*	*I $mA\ cm^{-2}$*	*% Current accountability*	
						AA	*HOAc*
145	3 M H_2SO_4	0.27	1.1	276	17.6	25	61
	1.5 M H_2SO_4	0.35	0.9	278	13.3	27	64
150	1 M H_2SO_4	0.6	0.9	208	18.9	32	72
147	1 M H_2SO_4	0.5	1.0	267	18.2	32	66
148	1 M $HClO_4$	0.6	1.0	274	17.5	30	81

Dissolved ethanol concentration is 0.5 M in anolyte feed. See Table 2 for explanation of symbols and other details.

Table 4. Selected steady state data for alcohol oxidation at the packed bed anode

Expt.	*[ROH]*	*Cell R (Ω)*	*Anolyte flow cm³ min⁻¹*	*Cell E (mV)*	*Anode E (mV w.r.t. RHE)*	*I mA cm⁻²*	*% Current accountability*	
							A	*Acid*
150	0.5 M EtOH	0.6	0.8	267	613	13.6	34	52
			0.9	208	663	18.9	32	72
154	0.5 M 2-propanol	0.45	1.0	267	613	13.5	96	0
			0.9	207	666	17.2	108	0

See Table 2 for details; here A = acetaldehyde (from ethanol) or acetone (from 2-propanol). Electrolyte was 1 M H_2SO_4.

major difference in selectivity behaviour for oxidation of primary and secondary alcohols as observed here and suggests the possibility of general special selectivity in oxidation of secondary alcohols.

Since oxidation of 2-propanol to acetone is a two-electron transfer, while ethanol to acetic acid involves four electrons, the platinum–graphite anode was actually more active in the secondary alcohol when considered in terms of alcohol turnover frequencies. The frequencies calculated from Table 4 for 2-propanol are 0.064 and 0.082 s^{-1} which can be compared with the earlier value of 0.06 s^{-1} for ethanol.

4.7. *Effect of product accumulation*

Another aspect of alcohol oxidation in packed bed anodes which was selected for brief examination involved the effect of product accumulation on reaction rate. In future applications of these electrogenerative processes, high conversions will probably be a goal. Under these conditions, the concentration of the oxidation products would be substantial. Other workers [18] have observed that acetic acid inhibits the oxidation of dissolved ethanol on platinum. Thus, some experiments were conducted to explore this possibility in the reactor featuring the graphite-supported platinum packed bed anode and both primary and secondary alcohols.

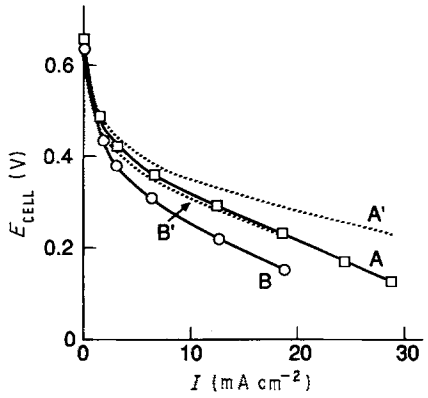

Fig. 6. Effect of acetic acid addition to the anolyte on IR-corrected polarization curves for electrogenerative oxidation of 0.5 M dissolved ethanol (1 $cm^3 min^{-1}$) in a Pt-graphite sheet packed bed. Electrode area = 6.45 cm^2, LAA-2 oxygen cathode, T = 25°C, Cell R = 0.51–0.6 Ω. Divided cell (R-4010 membrane). Curves A, A′ (Expt. 147): without added acetic acid, 1 M H_2SO_4 electrolyte. Curves B, B′ (Expt. 148): with 0.1 M acetic acid added to the anolyte, 0.9 M H_2SO_4 electrolyte. Curves A, B: observed potentials. Curves A′, B′: with IR correction.

In Fig. 6, the effect of acetic acid addition to the anolyte is demonstrated. The anolyte was 1 M H_2SO_4 with 0.5 M dissolved ethanol reactant. Cell performance without addition of acetic acid is shown in Curve A. When acetic acid was added to the anolyte (to obtain 0.1 M CH_2COOH concentration), the cell performance was diminished somewhat to that shown in Curve B.

A similar experiment was performed with acetone addition for 2-propanol oxidation. Curve B of Fig. 5 shows cell performance with the addition of acetone to the 0.1 M level in the anolyte. The difference between Curves A and B confirms inhibition by the acetone. Although this investigation of the packed bed reactor for oxidation of dissolved alcohol focused on demonstrating feasibility of operation, future catalyst studies may need to address the problem of product inhibition if operation at high conversions or recycle is desired.

4.8. *Effects of membrane transfer*

While some of the calculated total current accountabilities in Tables 2 through 4 in excess of 100% can be explained by experimental error, this tendency occurred too frequently to be ascribed only to the analytical procedures. The transfer of oxygen through the membrane to react with the dissolved organics in the anolyte or alcohol to react with oxygen at the cathode would result in chemical reaction without electric current generation. This is effectively 'chemical shorting'. Although the thin modified perfluorinated ion exchange membrane was supposed to minimize possibilities for 'chemical shorting' through the cell, some undoubtedly occurred to various degrees via the two mechanisms.

For 'chemical shorting' to occur through organic transport, ethanol or acetaldehyde would diffuse across the ion exchange membrane that separates the electrodes, react at the catalytic cathode to acetic acid and diffuse back to the anolyte. HPLC analysis of the catholyte from some of the experiments described earlier confirmed the presence of acetic acid there. The average concentration was approximately 1 mg ml^{-1} acetic acid in a 10 ml sample.

To explore the acetic acid transport across the membrane more quantitatively, the reactor used in the

experiments above was again assembled in the usual manner, installed in the flow system and heated to 40° C. Static catholyte and flowing anolyte (both 3 M H_2SO_4) were employed with the RAI-4010 ion exchange membrane. No gases were passed over the electrodes. HPLC analysis of a sample of the flowing anolyte revealed no residual acetic acid from previous experiments. Acetic acid (1.2 mg ml^{-1}) was then added to the catholyte, and the anolyte was continuously sampled over a 20 min period. From HPLC analysis of these samples, the rate of transport of acetic acid across the membrane was calculated to be about 5×10^{-7} mol min^{-1} from the 1.2 mg ml^{-1} concentration in the catholyte. Similar experiments with the NAFION 117 ion exchange membrane and an American Cyanmid TA-1 Teflon matrix separator gave comparable results. Other investigations have also noted carboxylic acid transport through Nafion membrane [41]. Thus acetic acid transport from the catholyte could account for part of the high total current accountabilities.

The transport of oxygen across the ion exchange membranes employed here is possible since both the RAIPORE and NAFION membranes feature a sulphonated Teflon copolymer structure. The high solubility of oxygen in Nafion membranes compared with its solubility in aqueous solvents is known to enhance its diffusion rate and other workers [42, 43] have shown these types of membranes to be very permeable to oxygen. Thus, it is possible that oxygen from O_2-saturated catholyte can diffuse into the anolyte and react chemically with dissolved ethanol at the catalytic anode or with acetaldehye or other intermediates. Formation of peroxy acids and peroxy esters in chemical systems involving ethanol and acetaldehyde has been reported elsewhere [44, 45]. Such chemical reactions in the anolyte could also account for product formation, which would result in calculated current accountabilities exceeding 100%.

An experiment was conducted with the packed bed reactor to investigate this possibility further. Acetaldehyde (0.1 M) was dissolved in 1 M H_2SO_4 anolyte which flowed (0.8 ml min^{-1}) through the platinum–graphite packed bed anode. As usual, an LAA-2 gas diffusion oxygen cathode was employed opposite the packed bed. The separator was an RAI R-4010 ion exchange membrane. Polarization experiments produced limited current for acetaldehyde oxidation (< 5 mA cm^{-2}).

The cell was then operated at steady-state conditions with acetaldehyde with an IR corrected cell potential of 256 mV, a cell current density of 4 mA cm^{-2}, and a measured anode potential of 722 mV (RHE). Analysis of the anolyte from steady-state operation with HPLC resulted in a calculated current accountability for acetic acid of 114%. Acetic acid was the only observed product. This result shows that some direct oxidation of acetaldehyde product dissolved in the anolyte could play a role in explaining the larger total current accountabilities calculated in the experiments reported above.

With the experiments above, it was not possible to distinguish the relative contribution of the two possible transfer processes under our exploratory experimental conditions. However, both processes lead primarily to acetic acid and apparently represent only a minor contribution to the yield of that product when they do occur. They do not alter the general selectivity tendencies as can be seen from comparing Tables 1 and 2. However their contribution would be most evident at lower currents when smaller amounts of materials are generated electrochemically and at longer steady-state periods when organic acid could accumulate in the cathode compartment through which there was not always electrolyte flow. Note that although the chemical shorting discussed here does not produce current, at low levels it would not be detrimental in an electrogenerative reactor if acetic acid were a desired product.

5. Discussion

While most of our data are presented in terms of cell polarization to emphasize electrogenerative performance, Fig. 7 shows anode polarization with respect to the reversible hydrogen electrode for comparison with the literature. The data represent four polarizations under similar conditions from two separate experiments where a reference electrode was utilized. Table 5 compares the Tafel parameters from Fig. 7 with those from two other studies where true surface areas based on hydrogen electrosorption were reported. For a basis of comparison, exchange currents are taken at 220 mV (the thermodynamic equilibrium potential for ethanol/acetaldehyde [2]), scaled to ethanol concentration and based on apparent electrode area as well as on true Pt surface area. Although comparison of absolute catalytic reaction rates between laboratories is difficult, the agreement in the platinum-based exchange currents is quite good considering the variations and differences in the electrodes which were studied. Although slopes increased with potential in all instances the tabulated values represent best fits to

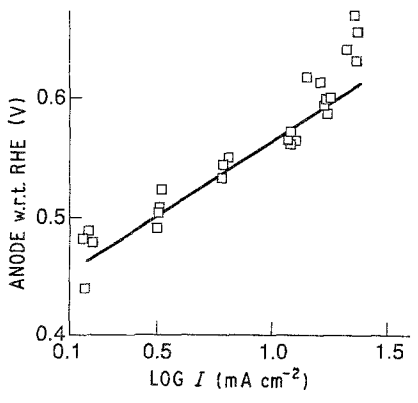

Fig. 7. Anode polarization w.r.t. RHE for electrogenerative oxidation of 0.25 M dissolved ethanol (1 cm^3 min^{-1}) in a Pt–graphite sheet packed bed. Electrode area = 6.45 cm^2, LAA-2 oxygen cathode, T = 25° C, Cell R = 0.5–0.6 Ω. Divided cell (R-4010 membrane) with 1 M H_2SO_4 electrolyte. Expts 171 and 172. Line represents i_0 = 0.011 mA cm^{-2}, slope = 115 mV decade^{-1} and E^0 = 220 mV.

Table 5. Comparison of Tafel parameters for ethanol oxidation on platinum anodes[a]

Electrode type	*Tafel slope* ($mV\,decade^{-1}$)	*Exchange current A/M–EtOH*		*Reference*
		Pt[b] ($A\,cm^{-2}$)	*Apparent* ($A\,cm^{-2}$)[b]	
Bright Pt	*115*	3×10^{-7}	5.0×10^{-7}	*[12]*
Platinized-Pt	*105*	2×10^{-7}	3.4×10^{-5}	*[22]*
Pt–graphite	*115*	1×10^{-7}	4.5×10^{-5}	*This work*

[a] *Data from 'steady-state' polarization in 0.5 or 1 M H_2SO_4 at 27° C.*
[b] *Normalized exchange current, see text.*

the respective data below 550 mV. Matsui *et al.* [18] normalized their currents to free Pt surface based on hydrogen codeposition and obtained Tafel plots that were linear from 300 to 450 mV. Their slopes of 133 mV decade^{-1} at 0° C would correspond to 146 mV decade^{-1} at 27° C if α remains constant.

The preceding observations on total current allow some conjecture about reaction mechanism in these relatively concentrated solutions. The observed Tafel slope of 120 mV decade^{-1} would be consistent with a single slow electron transfer reaction as the rate determining step in the region below 600 mV (RHE). That observation together with some dependence of current on ethanol concentration suggests the first electron transfer as the rate determining step (r.d.s.). The increasing Tafel slope observed above 600 mV may be explained as a change in r.d.s. to a preceding adsorption step or perhaps pore diffusion at higher currents when charge transfer is sufficiently accelerated. Blocking by surface oxide may be proposed to explain the end of the Tafel region, but it should not be significant below 800 mV (see, for example, [15]). Similarly, mechanisms involving surface hydroxyl groups in the oxidation step [25] seem unlikely given that acetaldehyde production begins as low as 350 mV [19], although mechanisms may change with potential. Also, the hydroxyl mechanism cannot explain the 133 mV Tafel slope together with the first order dependence on ethanol concentration in the free surface-based data of Matsui *et al.* [18].

With successful operation of the electrogenerative reactor, product selectivity is perhaps of greater interest than cell polarization and can provide some further insights into reaction mechanisms. While carbon dioxide production can account for 20% or more of total current at gas diffusion electrodes fed with vaporized ethanol from aqueous solutions [2], we found that acetaldehyde and acetic acid accounted for about all of the current at liquid-fed packed beds. Acetic acid production was favoured over acetaldehyde in the Pt–graphite packed bed relative to the platinum-black–Teflon composite electrode (AA-1) bed and was found to increase with ethanol concentration. We also found that both significant concentrations of preformed acetic acid and acetaldehyde apparently inhibit ethanol oxidation. Heitbaum *et al.* [19] found CO_2 as a major product using relatively dilute, dissolved ethanol (0.01 M) at gas-diffusion-type anodes used in their differential electrochemical mass spectroscopy experiments. Podlovchenko *et al.* [46] found carbon dioxide accounted for 2% or less of current when purging an inert gas through the electrolyte while oxidizing dissolved ethanol (0.5 M) at a platinum electrode. Other workers who analysed products found only acetaldehyde and acetic acid at ratios that varied with catalyst type and experimental conditions [11, 18, 46, 47].

The observations above including selectivity data enable us to postulate a general scheme for the reaction mechanism together with an explanation of products as shown in Fig. 8. Our observations, together with those of others [15, 22, 46, 47], that dissolved acetaldehyde is only slowly oxidized in the Tafel potential range would suggest a branching in the reaction network through a single adsorbed intermediate (*III*) so that acetic acid and acetaldehyde are produced in parallel rather than in series. Selectivity could be determined by relative reaction rates of $CH_3\overset{*}{C}HOH$ (*III*) between the two alternative routes to desorption. Involved are competitive adsorption between ethanol (the predominant adsorbing species) and surface adsorbed intermediates. Steps preceding hydrogen ion formation are probably quasi-reversible in that adsorbed hydrogen, H^-*, is formed together with intermediate species such as (*V*) and (*VI*). Furthermore, significant water of hydration must be present

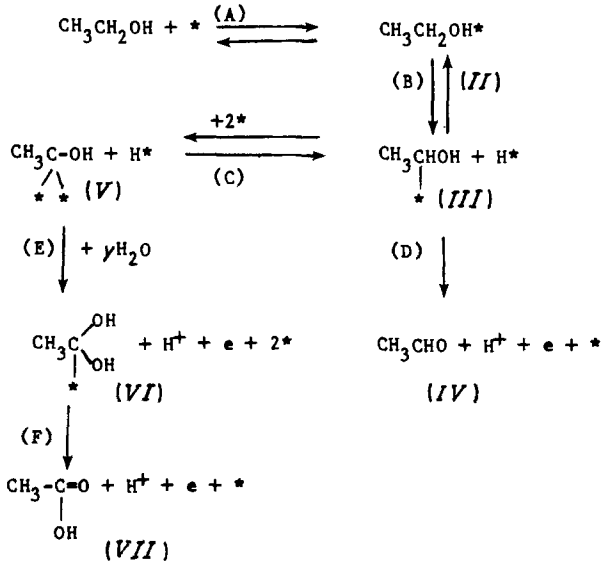

Fig. 8. Postulated general reaction network for ethanol oxidation at platinum anodes. Adsorbed hydrogen atoms can react at any time with water to give ions plus electrons: H^-* + $xH_2O \rightarrow H^+$ (hydrated) + * + e.

for release of protons and other steps [1]. The presence of dispersed hydrophobic surface Teflon limits the availability of water for hydration although it does not eliminate it. With hydrophobic material in proximity the competition for adsorption is between adsorbed intermediate and ethanol. Acetaldehyde may not be hydrated at the surface. Thus, step B can take place in concert with step D to give acetaldehyde and several protons. With significant water present at the surface (in the absence of a hydrophobic treatment) more hydrogen atoms are hydrated and acetic acid is formed. This can be explained by Reaction 5 which involved hydration and surface water. Routes with the highest overall rate constants will be favoured. Limited surface water may favour route D especially since *III* must dissociate further to give *V*. The supply of fresh ethanol molecules in the flow system probably facilitates desorption of reactive intermediates:

$$\underset{*}{\underset{|}{CH_3CHOH}} \underset{-2^*}{\overset{+2^*}{\rightleftharpoons}} \underset{* \quad *}{CH_3C\text{–}OH} + H^-{}^*$$

(*III*) (*V*)

$$+ xH_2O$$

$$\underset{*}{\underset{|}{CH_3C\text{–}(OH)_2}} + 2^* + 2H^+(\text{hydrated}) + 2e$$

(*VI*) (5)

The complete oxidation of ethanol and formation of carbon dioxide on hydrophobic treated electrodes often in the presence of lower concentrations of ethanol can be rationalized in terms of further dissociation of intermediates such as *V* or *VI* with formation of complex carbonaceous species with $H^-{}^*$. These species require arrays of surface sites. They eventually interact with water to give protons plus current (electrons), for example

$$\underset{*}{\underset{|}{CH_3C(OH)_2}} + 2^* \longrightarrow \underset{* \quad *}{CH_2\text{–}C\begin{matrix}OH\\OH\end{matrix}} + H^*$$

(*VI*)

$$\longrightarrow \cdots + H_2O \longrightarrow CO_2 + H^+ \text{ (hydrated)} + e$$

(6)

The increased tendency for acetic acid formation in the presence of a large excess of ethanol may be explained by acetyl formation as suggested by Wilsau and Heitbaum [19, 20] or through ethanol interaction with *V*, both of which can give ethyl acetate. Ethyl acetate could then by hydrolysed to acetic acid upon desorption into the strong acid electrolyte. This, however, is only one possibility. The reaction scheme suggested here does not preclude the existence of some other parallel routes suggested earlier.

The results obtained with isopropanol serve to confirm the general form of the mechanism we have proposed. Oxidation of a secondary alcohol led only to the ketone which is equivalent to the aldehyde for a primary alcohol. The reaction apparently proceeds via sequential dehydrogenation. To form a carboxylic acid from a secondary alcohol would require either carbon–carbon scission or oxidation of a methyl group. Neither of those proceses occurred at significant rates on the platinum–graphite packed bed anodes with dissolved substrate in the potential range used for electrogenerative oxidation. On the other hand, complete oxidation to carbon dioxide is possible in the vapour state.

Acknowledgement

We thank Dr. Michael Foral for help with electrochemical platinum surface area measurements and Liliana Concari, Milton Stewart, Steve Sitkiewitz and Douglas Dolan for help with cell operation and analytical procedures. RAI Research Corporation provided membranes for cell dividers. We also thank the National Science Foundation and the University of Wisconsin for support of this work.

Appendix

Solution phase potential drop

Potential and concentration distributions in a flow-by packed bed well below the limiting current have been treated by Alkire and Ng [48], but even with some simplifying assumptions their equations in cylindrical coordinates require a numerical solution which is not directly applicable here. By assuming one-dimensional flow of ionic current in the direction perpendicular to the plane of the electrode and treating the surface current distribution as uniform in all directions, we can estimate the maximum electrolyte-phase potential drop at a given current density in our flat packed bed. These assumptions are justified at the low conversions employed in this study. Moreover, treating the surface current distribution as uniform in the direction of ionic current flow should ensure that an upper-limit potential drop is determined.

For this case, Ohm's law and a charge balance lead to a one-dimensional second order differential equation which can be integrated to yield the potential difference between electrolyte at the front (cathode side) and back of the electrode

$$\Delta\Phi = \frac{id}{2\kappa} \tag{A1}$$

where i is the current density at the front of the electrode, d is the electrode thickness and κ is the conductivity of the electrolyte in the pores of the packed bed. That result is equivalent to the low conversion case in the limiting current analytical solution of Risch and Newman [49] when the mass-transfer-controlled current density in their expression is replaced by the observed current density which, in our case, is determined by kinetics.

We can evaluate $\Delta\Phi$ in Equation A1 for our higher observed current density of 25 mA cm^{-2} in the platinum–graphite packed bed with a conductivity of 0.091 Ω^{-1} cm^{-1} calculated from the Bruggemann Equation for 1 M H_2SO_4 and a porosity of 0.4. The result is a maximum potential difference of 44 mV. The effect of polarization on reaction rate would be expected to reduce that potential difference by redistributing the current. An upper limit to redistribution can be calculated from the maximum potential drop and the observed Tafel slope of 120 mV decade^{-1}. We can conclude that the overpotential could be reduced by at most 44 mV, and that the ethanol reaction rate could be up to 60% lower at the back of the anode relative to the front, under the experimental conditions described here.

References

[1] R. L. Pesselman, T. M. Meshbesher, S. Floyd and S. H. Langer, *Chem. Engng Commun.* **38** (1985) 265.
[2] S. H. Langer, J. C. Card and M. J. Foral, *Pure Appl. Chem.* **58** (1986) 895.
[3] B. O. Palsson, S. Fathi-Afshar, D. F. Rudd and E. N. Lightfoot, *Science* **213** (1981) 513.
[4] K. Park, P. N. Pintauro, M. M. Baizer and K. Nobe, *J. Electrochem. Soc.* **132** (1985) 1850.
[5] C. Oloman and A. P. Watkinson, *Can. J. Chem. Engng* **54** (1976) 312.
[6] F. Goodridge and M. A. Hamilton, *Electrochim. Acta* **25** (1980) 481.
[7] R. C. Alkire and R. M. Gould, *J. Electrochem. Soc.* **127** (1980) 605.
[8] M. W. Breiter 'Electrochemical Processes in Fuel Cells', Springer New York (1969).
[9] W. Vielstich, 'Fuel Cells', Wiley, New York (1970).
[10] G. Sundholm, *J. Electroanal. Chem.* **31** (1971) 265.
[11] R. A. Rightmire, R. L. Rowland, D. L. Boos and D. L. Beals, *J. Electrochem. Soc.* **111** (1964) 242.
[12] A. R. Blake, A. T. Kuhn and J. G. Sunderland, *ibid.* **120** (1973) 492.
[13] H. Matsui, T. Terazawa and T. Hisano, *Nippon Kagaku Kaishi* **10** (1974) 1861.
[14] K. V. Rao, *J. Electrochem. Soc. India* **27** (1978) 211.
[15] S. N. Raicheva, S. V. Kalcheva, M. V. Christov and E. I. Sokolova, *J. Electroanal. Chem.* **55** (1974) 213.
[16] S. V. Kalcheva, M. V. Christov, E. I. Sokolova and S. N. Raicheva, *ibid.* **55** (1974) 231.
[17] *Idem, ibid.* **55** (1974) 223.
[18] H. Matsui, T. Hisano and T. Terazawa, *Nippon Kagaku Kaishi* **5** (1983) 618.
[19] J. Willsau and J. Heitbaum, *J. Electroanal. Chem.* **194** (1985) 27.
[20] *Idem, Electrochim. Acta* **31** (1986) 943.
[21] B. Beden, M.-C. Morin, F. Hahn and C. Lamy, *J. Electroanal. Chem.* **229** (1987) 353.
[22] K. V. Rao and C. B. Roy, *J. Indian Chem. Soc.* **54** (1977) 1180.
[23] E. Sokolova, *Electrochim. Acta* **20** (1975) 323.
[24] K. D. Snell and A. G. Keenan, *ibid.* **27** (1982) 1683.
[25] *Idem, ibid.* **26** (1981) 1339.
[26] M. V. Christov and E. I. Sokolova, *J. Electroanal. Chem.* **175** (1984) 183.
[27] S. N. Raicheva, M. V. Christov and E. I. Sokolova, *Electrochim. Acta* **26** (1981) 1669.
[28] C. Liang and T. C. Franklin, *ibid.* **9** (1964) 517.
[29] G. Horanyi, P. Konig and I. Telcs, *Acta Chim. (Budapest)* **72** (1972) 165.
[30] K. V. Rao and C. B. Roy, *Indian J. Chem.* **19A** (1980) 840.
[31] E. I. Sokolova and M. V. Christov, *J. Electroanal. Chem.* **175** (1984) 195.
[32] T. M. Meshbesher, US Pat. No. 4 347 109 (August 31, 1982).
[33] R. G. Haldeman, W. P. Colman, S. H. Langer and W. A. Barber, *Adv. Chem. Ser.* **47** (1965) 106.
[34] H. P. Landi, US Pat. 3 527 616 (1970).
[35] J. C. Card, M. J. Foral and S. H. Langer, *Environ. Sci. Technol.* **22** (1988) 1499.
[36] E. Mentasti, M. C. Gennaro, C. Sarzanini, C. Balocchi and M. Savigliano, *J. Chromatogr.* **322** (1985) 177.
[37] R. W. McCabe and P. J. Mitchell, *Ind. Engng Chem. Prod. Res. Dev.* **23** (1984) 196.
[38] R. W. McCabe, C. L. DiMaggio and R. J. Madix, *J. Phys. Chem.* **89** (1985) 854.
[39] C. N. Satterfield, 'Mass Transfer in Heterogeneous Catalysis', MIT Press, Cambridge, Mass. (1970).
[40] E. J. Wilson and C. J. Geankoplis, *Ind. Engng Chem. Fund.* **5** (1966) 9.
[41] H. L. Chum, A. K. Hauser and D. W. Sopher, *J. Electrochem. Soc.* **130** (1983) 2507.
[42] Z. Ogumi, Z. Takehara and S. Yoshizawa, *J. Electrochem. Soc.* **131** (1984) 769.
[43] Z. Ogumi, T. Kuroe and Z. Takehara, *ibid.* **132** (1985) 2001.
[44] A. Streitwieser and C. H. Heathcock, 'Introduction to Organic Chemistry', MacMillan, New York (1976).
[45] D. Swern (Ed.), 'Organic Peroxides', Vol. 1, Wiley, New York (1969).
[46] B. I. Podlovchenko, T. D. Gladysheva, V. F. Stenin and V. I. Levina, *Sov. Electrochem.* **9** (1973) 1579.
[47] V. M. Hollnagel and U. Lohse, *Z. Physik. Chem.* **232** (1966) 237.
[48] R. Alkire and P. K. Ng, *J. Electrochem. Soc.* **121** (1974) 95.
[49] T. Risch and J. Newman, *ibid.* **131** (1984) 2551.